JACS
JOURNAL OF THE AMERICAN CHEMICAL SOCIETY
Article
Cite This: J. Am. Chem. Soc. 2019, 141, 922–927
pubs.acs.org/JACS

Kinetics of the Topochemical Transformation of $(PbSe)_m(TiSe_2)_n(SnSe_2)_m(TiSe_2)_n$ to $(Pb_{0.5}Sn_{0.5}Se)_m(TiSe_2)_n$

Duncan R. Sutherland,[†] Devin R. Merrill,[†] Jeffrey Ditto,[†] Daniel B. Moore,[†] Douglas Medlin,[‡] and David C. Johnson*[,†]

[†]Materials Science Institute and Department of Chemistry and Biochemistry, University of Oregon, Eugene, Oregon 97403, United States

[‡]Sandia National Laboratories, Livermore, California 94551, United States

ABSTRACT: Solid-state reaction kinetics on atomic length scales have not been heavily investigated due to the long times, high reaction temperatures, and small reaction volumes at interfaces in solid-state reactions. All of these conditions present significant analytical challenges in following reaction pathways. Herein we use in situ and ex situ X-ray diffraction, in situ X-ray reflectivity, high-angle annular dark field scanning transmission electron microscopy, and energy-dispersive X-ray spectroscopy to investigate the mechanistic pathways for the formation of a layered $(Pb_{0.5}Sn_{0.5}Se)_{1+\delta}(TiSe_2)_m$ heterostructure, where m is the varying number of $TiSe_2$ layers in the repeating structure. Thin film precursors were vapor deposited as elemental-modulated layers into an artificial superlattice with Pb and Sn in independent layers, creating a repeating unit with twice the size of the final structure. At low temperatures, the precursor undergoes only a crystallization event to form an intermediate $(SnSe_2)_{1+\gamma}(TiSe_2)_m(PbSe)_{1+\delta}(TiSe_2)_m$ superstructure. At higher temperatures, this superstructure transforms into a $(Pb_{0.5}Sn_{0.5}Se)_{1+\delta}(TiSe_2)_m$ alloyed structure. The rate of decay of superlattice reflections of the $(SnSe_2)_{1+\gamma}(TiSe_2)_m(PbSe)_{1+\delta}(TiSe_2)_m$ superstructure was used as the indicator of the progress of the reaction. We show that increasing the number of $TiSe_2$ layers does not decrease the rate at which the $SnSe_2$ and PbSe layers alloy, suggesting that at these temperatures it is reduction of the $SnSe_2$ to SnSe and Se that is rate limiting in the formation of the alloy and not the associated diffusion of Sn and Pb through the $TiSe_2$ layers.

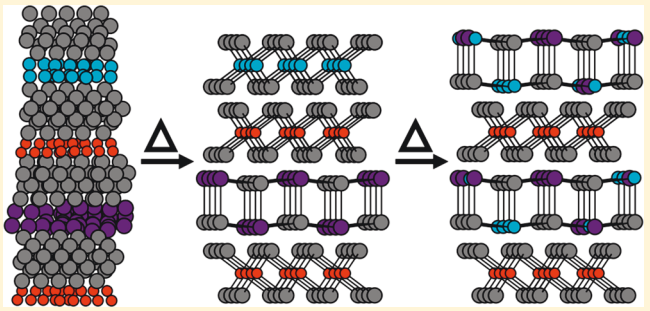

INTRODUCTION

Understanding the kinetics of solid-state reactions is particularly important in the formation of metastable phases, but it is challenging to obtain detailed information about most solid-state reactions because reactants are typically powders and the reactions and structural changes occur at the many surfaces and interfaces. Solid-state reactions are typically monitored by tracking changes in unit cell volume,[1] by tracking the ratio of reactants and products and their structural evolution using Rietveld refinement of diffraction data,[2−4] or via in situ electron microscopy and electron diffraction studies.[5] In situ X-ray diffraction techniques have been used to probe solid-state reactions[6,7] and more complex synthesis methods such as solvothermal approaches.[8,9] Combining in situ scattering and spectroscopy techniques has also provided useful insights into reaction pathways.[10,11] Obtaining direct information about the atomic level steps in solid-state reactions, however, remains elusive due to the heterogeneous nature of reactions occurring at interfaces.

Topotactic reactions via soft chemical reactions are often used to form metastable compounds. Topotactic reactions are those where a structural change occurs where the final structure is related to the initial structure through crystallographic orientation. There may be a loss or gain of atoms during the transition, and structural units of the original structure may be maintained during the reaction. The preservation of basic structural features between reactants and products constrains possible reaction pathways. The most common examples of topotactic reactions are intercalation and ion exchange. These reactions are of vital importance for battery applications, where the commercial technology depends on the reversibility of the topotactic reactions.[12,13] Other topotactic reactions of interest include intercalation of large organic molecules into layered clay structures for sensing applications,[14] transition metal oxide reductions,[1] and the redox synthesis of metastable magnetic phases.[4] Layered compounds, because of the obvious diffusion pathways parallel to the layers and preferred orientation that enhances reflection intensities in diffraction experiments, are particularly attractive for in situ studies of topotactic reactions. These investigations have resulted in proposed reaction mechanisms, such as the intercalation of Li into TiS_2.[15−17] Although diffusion is easy parallel to the layers, what happens perpendicular to the layers is less obvious and yet is critical to accomplishing transformations that require mass exchange between the layers.

Received: October 3, 2018
Published: December 17, 2018

DOI: 10.1021/jacs.8b10681
J. Am. Chem. Soc. 2019, 141, 922–927

More challenging are studies of topochemical reactions in three-dimensional solids, and there is considerable interest in understanding the mechanism of these reactions due to their importance in lithium batteries.[18] The mechanistic understanding of intercalation reactions has enabled their use in multistep reactions which can be performed sequentially to accomplish transformations that cannot be done in a single one-step reaction.[3] Recent advances in preparing designed heterostructures through stacking of two-dimensional layers provide a new and diverse set of interesting starting materials for topochemical transformations.

In this paper we explore the conversion of ordered $(PbSe)_m(TiSe_2)_n(SnSe_2)_m(TiSe_2)_n$ superstructures into $(Pb_{0.5}Sn_{0.5}Se)_m(TiSe_2)_n$ at elevated temperatures using both diffraction and scanning transmission electron (STEM) techniques. The starting phases, $(PbSe)_1(TiSe_2)_n$-$(SnSe_2)_1(TiSe_2)_n$ where n = 1 and 3, enable us to create a sample with an abrupt concentration gradient where there is no mixing of Pb and Sn across a known distance of 0.6 or 1.8 nm, respectively. The monoselenides in both the precursor and product have distorted rock salt structures. The dichalcogenides in the precursor and product have the CdI_2 structure. The c-axis of the dichalcogenide is perpendicular to the substrate and the (100) plane of the rock salt structure. The topotactic nature of this reaction, illustrated schematically in Figure 1, combined with the preferred orientation of both the

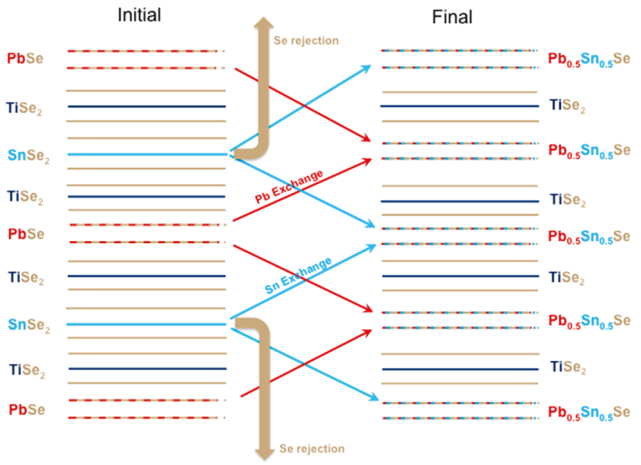

Figure 1. Schematic of the conversion of $(PbSe)_m(TiSe_2)_n(SnSe_2)_m$-$(TiSe_2)_n$ into $(Pb_{0.5}Sn_{0.5}Se)_m(TiSe_2)_n$, which involves the loss of Se and the interdiffusion of Sn and Pb through the intervening $TiSe_2$ layers.

reactants and products makes this an ideal system to probe the interconversion using in situ X-ray diffraction. $(PbSe)_m(TiSe_2)_n(SnSe_2)_m(TiSe_2)_n$ superstructures can be prepared at low temperatures and $(Pb_xSn_{1-x}Se)_m(TiSe_2)_n$ random alloys can be prepared at elevated temperatures[19] by using starting precursors with different structures that mimic the composition variation along the c-axis. Both families of compounds are structurally well characterized using both X-ray diffraction (XRD) and electron microscopy techniques, with atomically abrupt interfaces between structurally distinct layers. The ability to systematically change the nanoarchitecture and interface density through the design of the precursors is an added advantage of this system, as it allows both interdiffusion of layers and diffusion within a layer to be independently probed as a rate-limiting step in the reaction pathway. Following the self-assembly of the initial precursor into $(PbSe)_m(TiSe_2)_n(SnSe_2)_m(TiSe_2)_n$ at low temperatures, the conversion between the compounds is consistent with a two-step reaction mechanism. $SnSe_2$ decomposes through the loss of Se and the simultaneous reduction of the Sn in $(PbSe)_m(TiSe_2)_n(SnSe_2)_m(TiSe_2)_n$ to form SnSe. The Sn and Pb cations immediately begin to intermix through the intervening $TiSe_2$ layers. The rate of the formation of the final $(Pb_{0.5}Sn_{0.5}Se)_m(TiSe_2)_n$ product does not depend on the number of $TiSe_2$ layers between the Sn and Pb constituents, indicating the rate-determining step is the loss of Se and concomitant reduction of Sn.

While this study involves a very specific decomposition mechanism, the quick interdiffusion of Pb and Sn across an intervening solid at the relatively low temperature of 250 °C is a surprising result. Typically solids need to be heated to ~2/3 of their melting points for significant diffusion to occur, as this temperature is required to create a significant concentration of defects. The temperature where diffusion is observed in this study is much lower than the melting points of the respective solids (1079 °C PbSe,[20] 874 °C SnSe,[21] or higher than 900 °C, $TiSe_2$[22]). The abrupt concentration gradient and the short diffusion distances enhance the diffusion rate. As pointed out by Persson, the amorphous state sets a limit on what compounds can be nucleated. Only compounds more stable than the amorphous state can form.[23] This study suggests a general strategy to obtain an amorphous solid at low temperatures is to prepare precursors with abrupt concentration gradients, which potentially can be accomplished by sequentially depositing elements in thin layers. Low-temperature annealing will mix the layers, and the compound that forms will be the easiest to nucleate.

EXPERIMENTAL SECTION

Precursor films that mimic the composition modulation of the target compounds were prepared by sequentially depositing elemental layers. The precursors were deposited in a custom-built high-vacuum physical vapor deposition system at pressures below 5×10^{-7} Torr. Pb, Sn, and Ti were deposited using electron beam guns, and Se was deposited using an effusion cell. Rates were maintained at 0.1−0.3 Å/s at the substrate using a quartz crystal microbalance (QCM) to monitor the rate and control the power of the electron beam sources. Elemental layers were deposited using a PC-controlled pneumatic shutter system to expose the substrate to the plume of each source until a calibrated thickness measured by the QCM was reached. The procedure to calibrate the deposition parameters has been described in detail previously.[24] Precursor films were annealed in a N_2 environment ($[O_2, H_2O] \leq 0.8$ ppm) for ex situ experiments.

Adjustments to deposition parameters during calibration were made using X-ray reflectivity (XRR) and diffraction (XRD) as well as compositional characterization from electron probe microanalysis (EPMA) using a method described elsewhere.[25] XRR, $\theta/2\theta$ XRD, and in situ measurements were performed on a Bruker D8 Discover diffractometer (Cu Kα radiation). In-plane XRD measurements were performed using a Rigaku SmartLab diffractometer (Cu Kα radiation). In situ measurements were conducted using an Anton-Parr hot stage on the D8, with N_2 gas flowing through the polyether ether ketone polymer housing to prevent oxidation. The scan time for the in situ measurements was 600 s.

High-angle annular dark field scanning transmission electron microscopy (HAADF-STEM) and energy-dispersive X-ray spectroscopy (EDX) experiments were conducted at Sandia National Laboratories, using an aberration-corrected FEI Titan G2 80-200 STEM equipped with a four-quadrant large-area EDS detector and at Pacific Northwest National Laboratory using a JEOL ARM 200CF S/TEM. The STEMs were operated at 200 keV.

DOI: 10.1021/jacs.8b10681
J. Am. Chem. Soc. 2019, 141, 922−927

RESULTS AND DISCUSSION

Precursors to $(PbSe)_m(TiSe_2)_n(SnSe_2)_m(TiSe_2)_n$ superstructures were prepared by depositing specific sequences of elemental layers to target a specific product following procedures described previously.[24] Pairs of elements (shown in the square brackets below) were calibrated to produce specific metal/selenium compositions. The ratios between the elemental layers were adjusted to obtain cation ratios that matched the expected lattice mismatches. A [Pb|Se][Ti|Se][Sn|Se][Ti|Se] sequence of elemental layers was deposited as a precursor to the $(PbSe)_1(TiSe_2)_1(SnSe_2)_1(TiSe_2)_1$ superstructure. A second precursor was prepared by depositing three [Ti|Se] elemental bilayers twice in the same sequence of bilayers as a precursor for the $(PbSe)_1(TiSe_2)_3$-$(SnSe_2)_1(TiSe_2)_3$ superstructure.

A sequence of diffraction patterns was collected as a function of time while the annealing temperature was held constant at 275 °C, and the resulting data for the $(PbSe)_1(TiSe_2)_1$-$(SnSe_2)_1(TiSe_2)_1$ precursor are shown in Figure 2. The

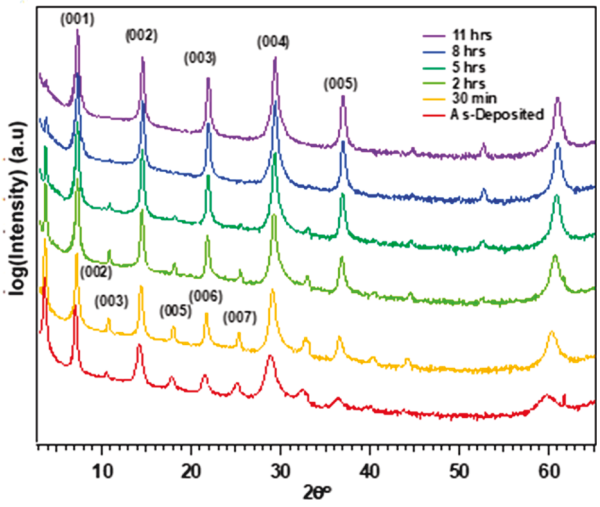

Figure 2. Specular diffraction patterns of a precursor to $(PbSe)_1(TiSe_2)_1(SnSe_2)_1(TiSe_2)_1$ obtained as a function of annealing time at 275 °C. The initial formation of $(PbSe)_1(TiSe_2)_1$-$(SnSe_2)_1(TiSe_2)_1$ is followed by its conversion into $(Pb_{0.5}Sn_{0.5}Se)_1(TiSe_2)_1$. The scans have been offset from one another for clarity.

sharpening of all peaks as well as an increase in intensity of the odd integer reflections in the 30 min scan indicates that a superstructure with the period of the precursor has self-assembled. The scan after 2 h shows decreases in the intensity of odd order reflections with increases in the even order reflection intensities, suggesting that the superstructure has begun to transform into the $(Pb_{0.5}Sn_{0.5}Se)_1(TiSe_2)_1$ final product. This transformation continues with time, with the odd order reflections systematically decreasing in intensity until only the (001) reflection of the original superstructure is barely visible after 11 h, while the even order reflections of the initial product grow in intensity (for example the (0014) reflection of the initial product, which is equivalent to the (007) reflection of the final product). Along with the changes in intensity, there is a slight shift of the reflections to higher angle as a function of time, suggesting a slight decrease in the unit cell size. After additional annealing, only the even order reflections remain, suggesting that the *c*-axis lattice parameter has been decreased by a factor of 2, which is consistent with the formation of $(Pb_{0.5}Sn_{0.5}Se)_1(TiSe_2)_1$. The relative intensities and the lattice parameter are consistent with that obtained for the compound $(Pb_{0.5}Sn_{0.5}Se)_1(TiSe_2)_1$ prepared without forming the three-component superstructure as a precursor.[19]

In-plane diffraction data collected as a function of annealing time is shown in Figure 3. All the reflections in the in-plane

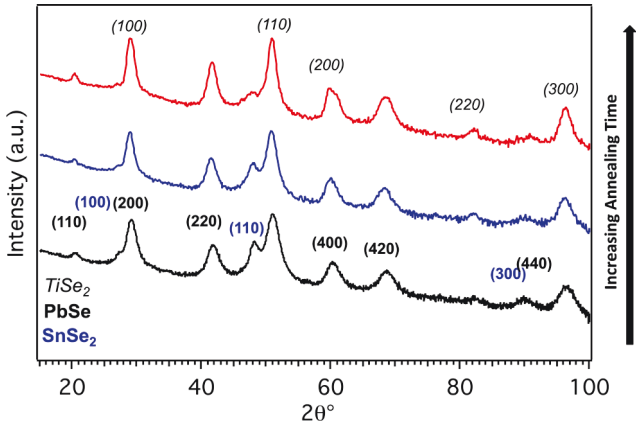

Figure 3. In-plane diffraction data as a function of annealing time at 275 °C (black = 30 min, blue = 2 h, red = 8 h.). The initial compound formed, $(PbSe)_1(TiSe_2)_1(SnSe_2)_1(TiSe_2)_1$, converts into $(Pb_{0.5}Sn_{0.5}Se)_1(TiSe_2)_1$ on annealing. The scans have been offset from one another for clarity.

diffraction pattern of the superstructure can be indexed as belonging to either $SnSe_2$, PbSe, or $TiSe_2$. There is no evidence for SnSe, which shows a strong distortion in the *a* and *b* lattice parameters of the rock salt structure.[19] As a function of time, the reflections for $SnSe_2$ lose intensity, as seen by the change in intensity of the (110) reflection at $2\theta \approx 47°$. The rock salt reflections appear, grow in intensity, slightly shift their position, and begin to broaden, suggesting a distortion of the in-plane structure is occurring. This is consistent with the formation of two layers each containing a $Pb_xSn_{1-x}Se$ alloy as a function of annealing time.[19] The in-plane diffraction data support the formula $(PbSe)_1(TiSe_2)_1(SnSe_2)_1(TiSe_2)_1$ for the initial superstructure formed and the sequence of events inferred from the 00l diffraction data. In the conversion of $(PbSe)_1(TiSe_2)_n(SnSe_2)_1(TiSe_2)_n$ into the final $(Pb_{0.5}Sn_{0.5}Se)_1(TiSe_2)_n$ compound, Se must diffuse out of the structure and Pb and Sn must exchange through the intervening $TiSe_2$ layers.

HAADF-STEM data were collected on a sample of $(PbSe)_1(TiSe_2)_3(SnSe_2)_1(TiSe_2)_3$. A representative image (Figure 4) contains a repeating sequence of a bright PbSe bilayer, three consecutive dark $TiSe_2$ trilayers, an intermediate intensity $SnSe_2$ trilayer, and a second band of three consecutive dark $TiSe_2$ trilayers. The structure of the bright PbSe bilayers is consistent with a rock salt structure in the areas oriented down a zone axis, agreeing with STEM images of other compounds containing a rock salt structured PbSe bilayer.[19] The structure of the $SnSe_2$ layer determined from the zone axis images is consistent with layers in the bulk CdI_2 structure, with Sn in an octahedral coordination centered between two Se layers. The structure of the $TiSe_2$ layers is consistent with the CdI_2 structure, where the outer Se layers octahedrally coordinate the middle Ti layer. The stacking of the $TiSe_2$ layers is mostly

DOI: 10.1021/jacs.8b10681
J. Am. Chem. Soc. 2019, 141, 922−927

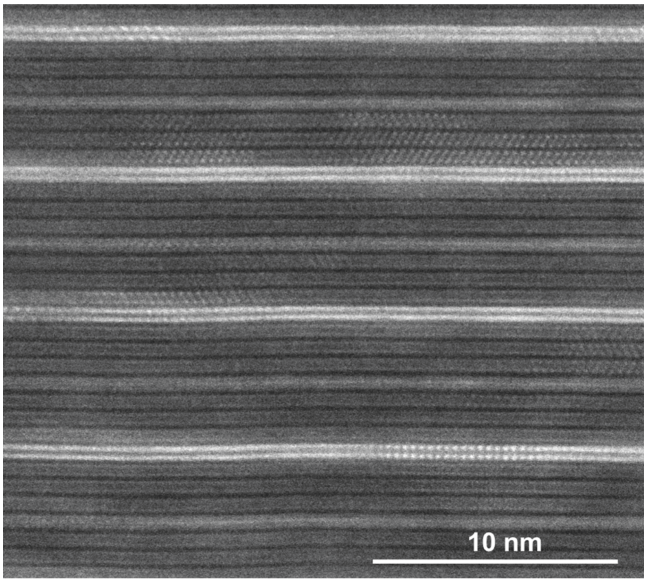

Figure 4. Representative HAADF-STEM image of $(PbSe)_1(TiSe_2)_3(SnSe_2)_1(TiSe_2)_3$ showing the atomically abrupt structural transitions between the constituent layers. The brightest layers are from the rock salt structured PbSe. The next brightest layer is from $SnSe_2$, and the three adjacent dark layers are $TiSe_2$.

consistent with the 1T polytype found for bulk $TiSe_2$, but occasionally a layer in the three-layer blocks has a different orientation than the other two. The STEM data are consistent with the observed specular and in-plane X-ray data, supporting the initial formation of the three component heterostructure, $(PbSe)_1(TiSe_2)_3(SnSe_2)_1(TiSe_2)_3$.

The topotactic nature of the observed transformation from $(PbSe)_1(TiSe_2)_1(SnSe_2)_1(TiSe_2)_1$ into $(Pb_{0.5}Sn_{0.5}Se)_1(TiSe_2)_1$ preserves the out-of-plane crystallographic alignment, making this system ideal for in situ diffraction measurements. Based on the data presented above, two different transformations are expected during the annealing. At low temperatures or for short times at higher temperatures, the precursor is expected to self-assemble into the ordered $(PbSe)_m(TiSe_2)_n$-$(SnSe_2)_m(TiSe_2)_n$ superstructure. At longer times or at higher temperatures, the $(PbSe)_m(TiSe_2)_n(SnSe_2)_m(TiSe_2)_n$ superstructure is expected to transform into the compound $(Pb_{0.5}Sn_{0.5}Se)_m(TiSe_2)_n$. To explore the self-assembly of the precursor into the ordered superstructure, XRR data were collected as a function of time at temperatures below 250 °C, as shown in Figure 5.

The intensity changes seen in Figure 5 as a function of time result from changing electron density in the repeating structure as it reorganizes to a more stable state with lower Gibbs free energy. The overall pattern changes very little, suggesting that there is minimal change in the overall superstructure. There is a slight shift in the position of the maxima of the first-order reflection and subsidiary maxima to higher angles as a function of time, indicating that the thickness of the deposited layers decreases. The shift corresponds to less than a 0.1% decrease in thickness and the peak also narrows, suggesting the sample is becoming more ordered. The second-order Bragg reflection does not shift position, which is consistent with the higher order reflections. This indicates that the second-order reflection results from the ordered superstructure. The relative positions of the first- and second-order Bragg reflections after annealing correspond more closely to that expected from

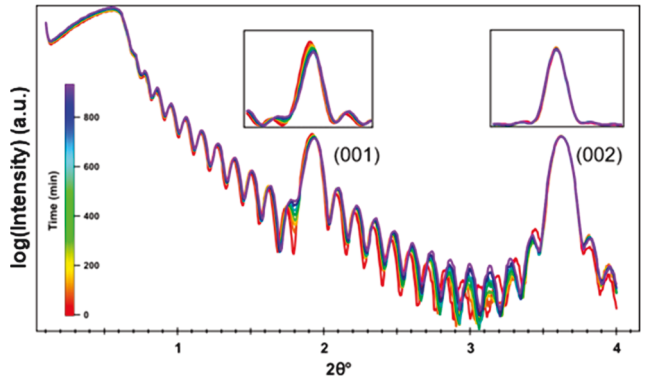

Figure 5. XRR data collected as a function of time at 150 °C. Each scan contains the first- and second-order Bragg reflections and a sequence of subsidiary maxima (Kissig fringes) resulting from the finite sample thickness and finite number of repeating sequences deposited in the initial reactant. The insets are expansions of the (001) and (002) reflections to make the small changes more apparent.

Bragg's law corrected for index of refraction changes. There is a slight decrease in the intensity of the first-order Bragg reflection, while the intensity of the second-order Bragg reflection remains constant. These changes suggest that annealing causes amorphous regions of the initially deposited samples to self-assemble into the ordered $(PbSe)_m(TiSe_2)_n$-$(SnSe_2)_m(TiSe_2)_n$ superstructure. The growth in intensity of the higher order odd Bragg reflections reflects the increased coherence as planes of atoms become regularly spaced. The intensity and position of the first-order Bragg reflection with time trends toward a constant value at low temperatures (Figures 6 and 7), which suggests that below 200 °C, $(PbSe)_m(TiSe_2)_n(SnSe_2)_m(TiSe_2)_n$ (where $m = 1$, $n = 1$ or $m = 1$, $n = 3$) compounds self-assemble from their respective precursors.

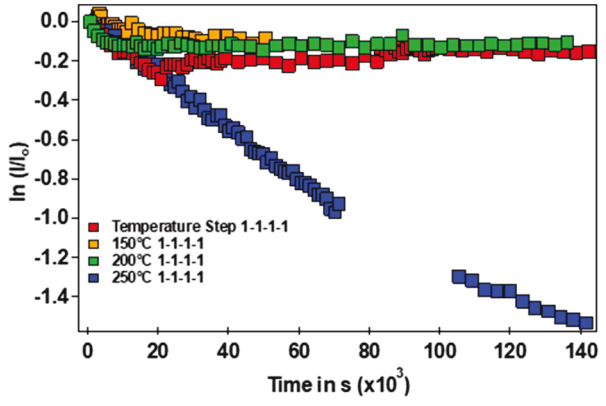

Figure 6. Variation of the natural logarithm of the normalized intensity of the (001) reflection as a function of annealing time and temperature. In the red data set, the sample was initially annealed at 250 °C for 3 h and then annealed at a reduced temperature of 200 °C and then 150 °C.

The change in the intensity of the first-order Bragg reflection is very different at higher temperatures, as shown in Figure 6. The intensity of the (001) reflection decreases continuously as a function of time for temperatures above 200 °C as the structure converts to the $(Pb_{0.5}Sn_{0.5}Se)_1(TiSe_2)_1$. If a sample is initially annealed for a period of time at 250 °C or higher and then the temperature is lowered below 200 °C, the (001)

DOI: 10.1021/jacs.8b10681
J. Am. Chem. Soc. 2019, 141, 922−927

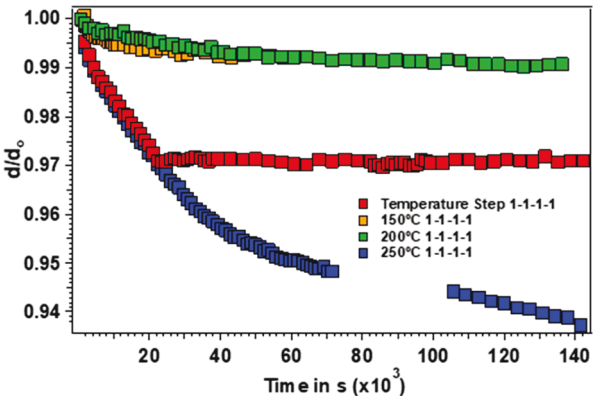

Figure 7. Change in normalized film thickness (d/d_0) as a function of time and temperature for an $m = 1$ $n = 1$ compound. In the red data set, the sample was initially annealed at 250 °C for 3 h and then annealed at a reduced temperature of 200 °C and then 150 °C.

reflection does not change in intensity as a function of time (red data set, Figure 6). This is consistent with the sample being a metastable mixture of $(PbSe)_m(TiSe_2)_n$-$(SnSe_2)_m(TiSe_2)_n$ and $(Pb_{0.5}Sn_{0.5}Se)_m(TiSe_2)_n$. This suggests that the conversion between these two structures is an activated process, requiring a temperature above 200 °C to have a measurable rate.

Figure 7 summarizes the changes in thickness as a function of annealing time and temperature for the same samples presented in Figure 6. The samples annealed at low temperatures all show a small decrease in thickness that trend to a constant value, with a change in the total thickness of less than 1%. This change reflects the structural rearrangements that occur during the self-assembly of $(PbSe)_1(TiSe_2)_1$-$(SnSe_2)_1(TiSe_2)_1$ from the mostly amorphous precursor. The samples annealed at higher temperatures show a much larger decrease in thickness, reflecting the larger changes that occur as $(PbSe)_1(TiSe_2)_1(SnSe_2)_1(TiSe_2)_1$ transforms into $(Pb_{0.5}Sn_{0.5}Se)_1(TiSe_2)_1$. At 250 °C the decrease in thickness is significantly faster than at lower temperatures. It decreases with increasing annealing time, perhaps reflecting the longer diffusion distances required for the Se that must be lost. A sample annealed for ~20 000 s at 250 °C and then annealed further at 200 or 150 °C has no change in sample thickness at the lower annealing temperatures. This suggests that higher temperatures are required to transform $(PbSe)_m(TiSe_2)_n$-$(SnSe_2)_n(TiSe_2)_n$ into $(Pb_{0.5}Sn_{0.5}Se)_m(TiSe_2)_n$. Se evaporates from the sample in this transformation, as confirmed using EPMA.

Considering the changes that must occur during the conversion of the $(PbSe)_m(TiSe_2)_n(SnSe_2)_n(TiSe_2)_n$ superstructure into the $(Pb_{0.5}Sn_{0.5}Se)_m(TiSe_2)_n$ alloy, there are two likely rate-limiting steps. One is the intermixing of Sn and Pb, which is being directly monitored by the previously discussed X-ray diffraction data. The second likely rate-limiting step is the reduction of Sn and concomitant loss of Se as the $SnSe_2$ converts into SnSe. To decouple these potential rate-limiting steps, annealing studies were performed on precursors with different thicknesses for the $TiSe_2$ layered regions separating the Sn and Pb containing layers. To first order, the reduction of Sn and loss of Se as the $SnSe_2$ converts into SnSe is expected to be independent of the thickness of the $TiSe_2$ layers. The increase in the thickness of the $TiSe_2$ region, however, increases the diffusion length for the mixing of Sn and Pb by a factor of 3. If interdiffusion is the rate-limiting step and if Fick's laws for diffusion hold, the thicker intervening $TiSe_2$ layers should decrease the interdiffusion rate of Sn and Pb by a factor of 9. If the diffusion does not follow Fick's laws, then the difference in the interdiffusion rates could be smaller or larger, but one would still expect it would take more time to diffuse a longer distance. Figure 8 contains the intensity of the (001)

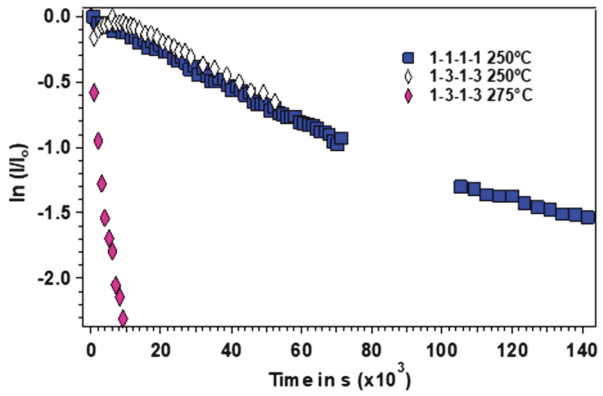

Figure 8. Decay of the intensity of the (001) reflection as a function of time and temperature for $(PbSe)_1(TiSe_2)_1(SnSe_2)_1(TiSe_2)_1$ and $(PbSe)_1(TiSe_2)_3(SnSe_2)_1(TiSe_2)_3$ samples at the indicated temperatures.

reflection versus time for $n = 1$ and $n = 3$ precursors when they are annealed at 250 °C. The decay in the intensity is the same for both, which indicates that the decomposition of $SnSe_2$ to SnSe and Se is the likely rate-limiting step in the reaction.

The diffraction and STEM studies are consistent with the following proposed mechanism:

$$\{m[PbI|Se]\}\{n[TiI(2+y)Se]\}\{m[SnI(2+y)Se]\}\{n[TiI(2+y)Se]\} \rightarrow (PbSe)_m(TiSe_2)_n(SnSe_2)_m(TiSe_2)_n \quad T \leq 200°C$$

$$(PbSe)_m(TiSe_2)_n(SnSe_2)_m(TiSe_2)_n \rightarrow (PbSe)_m(TiSe_2)_n(SnSe)_m(TiSe_2)_n + mSe \text{ (slow)}$$

$$(PbSe)_m(TiSe_2)_n(SnSe)_m(TiSe_2)_n \rightarrow (Pb_{0.5}Sn_{0.5}Se)_m(TiSe_2)_n \text{ (fast)} \quad T \leq 250°C$$

Since changing the thickness of the $TiSe_2$ layers does not change the rate of the reaction, the rate-limiting step of the higher temperature reaction is most likely the decomposition of $SnSe_2$ to SnSe. This decomposition requires the migration of Se out of the structure. The onset of the reaction at 250 °C and the associated decrease in film thickness suggest that this is the temperature required to decompose the $SnSe_2$ layer into SnSe and Se. The decomposition of $SnSe_2$ creates vacancies in the structure, which enable Se, Sn, and Pb atoms to diffuse through (or around) the $TiSe_2$ layers.

CONCLUSIONS

The data presented suggest that a topotactic reaction with multiple steps and identifiable intermediates occurs as precursors with defined nanoarchitecture evolve into specific $(Pb_{0.5}Sn_{0.5}Se)_m(TiSe_2)_n$ compounds. The precursors initially self-assemble into a three-constituent heterostructure, $(PbSe)_m(TiSe_2)_n(SnSe_2)_m(TiSe_2)_n$, when annealed briefly at higher temperatures or at lower temperatures for longer times. The values of m and n are defined by the nanoarchitecture of

DOI: 10.1021/jacs.8b10681
J. Am. Chem. Soc. 2019, 141, 922−927

the precursor. At elevated temperatures and longer annealing times, the structure rearranges to form $(Pb_{0.5}Sn_{0.5}Se)_m(TiSe_2)_n$, which maintains a layered architecture as the unit cell size decreases by a factor of 2 due to the now equivalent $(Pb_{0.5}Sn_{0.5}Se)_m$ layers. In this reaction, Sn is reduced, Se needs to diffuse out the film, and Pb and Sn need to diffuse through the intervening $TiSe_2$ layers. Since increasing the number of $TiSe_2$ layers (n) in the precursor, which increases the diffusion length, did not change the reaction rate, the decomposition of $SnSe_2$ into SnSe + Se is the rate-limiting step in the formation of $(Pb_{0.5}Sn_{0.5}Se)_m(TiSe_2)_n$ from the precursor.

AUTHOR INFORMATION

Corresponding Author

*davej@uoregon.edu

ORCID

David C. Johnson: 0000-0002-1118-0997

Notes

The authors declare no competing financial interest.

ACKNOWLEDGMENTS

The authors acknowledge support from the National Science Foundation under grant DMR-1710214. We acknowledge the use of instrumentation in the Center for Advanced Materials Characterization in Oregon (CAMCOR) at the University of Oregon. D.L.M. acknowledges support through Sandia National Laboratories, which is a multimission laboratory managed and operated by National Technology and Engineering Solutions of Sandia, LLC, a wholly owned subsidiary of Honeywell International, Inc., for the U.S. Department of Energy's National Nuclear Security Administration under contract DE-NA-0003525. We also acknowledge support through the Collaborative Access Team (CAT): Pooled Resources for Electron Microscopy Informatics, Education and Research (PREMIER) Network Program at Pacific Northwest National Laboratory (PNNL) and the Environmental Molecular Sciences Laboratory, a national scientific user facility sponsored by DOE's Office of Biological and Environmental Research at PNNL. PNNL is a multiprogram national laboratory operated by Battelle for DOE under contract DE-AC05-76RL01830.

REFERENCES

(1) Hernden, B. C.; Lussier, J. a.; Bieringer, M. Topotactic Solid-State Metal Hydride Reductions of Sr 2 MnO 4. *Inorg. Chem.* **2015**, *54* (9), 4249−4256.

(2) Neilson, J. R.; McQueen, T. M. Bonding, Ion Mobility, and Rate-limiting Steps in Deintercalation Reactions with ThCr 2Si 2-type KNi 2Se 2. *J. Am. Chem. Soc.* **2012**, *134* (18), 7750−7757.

(3) Masese, T.; Orikasa, Y.; Tassel, C.; Kim, J.; Minato, T.; Arai, H.; Mori, T.; Yamamoto, K.; Kobayashi, Y.; Kageyama, H.; et al. Relationship Between Phase Transition Involving Cationic Exchange and Charge-discharge Rate in Li2FeSiO4. *Chem. Mater.* **2014**, *26* (3), 1380−1384.

(4) Bridges, C. A.; Darling, G. R.; Hayward, M. a.; Rosseinsky, M. J. Electronic Structure, Magnetic Ordering, and Formation Pathway of the Transition Metal Oxide Hydride LaSrCoO3H0.7. *J. Am. Chem. Soc.* **2005**, *127*, 5996−6011.

(5) Streller, F.; Agarwal, R.; Mangolini, F.; Carpick, R. W. Novel Metal Silicide Thin Films by Design via Controlled Solid-State Diffusion. *Chem. Mater.* **2015**, *27*, 4247.

(6) Zhou, Y.; Pienack, N.; Bensch, W.; Patzke, G. R. The Interplay of Crystallization Kinetics and Morphology in Nanostructured W/Mo Oxide Formation: An in Situ Diffraction Study. *Small* **2009**, *5* (17), 1978−1983.

(7) Pienack, N.; Bensch, W. In-Situ Monitoring of the Formation of Crystalline Solids. *Angew. Chem., Int. Ed.* **2011**, *50* (9), 2014−2034.

(8) Zhou, Y.; Antonova, E.; Bensch, W.; Patzke, G. R. In Situ X-ray Diffraction Study of the Hydrothermal Crystallization of Hierarchical Bi_2WO_6 Nanostructures. *Nanoscale* **2010**, *2* (11), 2412−2417.

(9) Millange, F.; Medina, M. I.; Guillou, N.; Férey, G.; Golden, K. M.; Walton, R. I. Time-Resolved In Situ Diffraction Study of the Solvothermal Crystallization of Some Prototypical Metal-Organic Frameworks. *Angew. Chem., Int. Ed.* **2010**, *49* (4), 763−766.

(10) Kiebach, R.; Pienack, N.; Ordolff, M.; Studt, F.; Bensch, W. Combined In Situ EDXRD/EXAFS Investigation of the Crystal Growth of [Co (C6H18N4)][Sb2S4] Under Solvothermal Conditions : Two Different Reaction Pathways Leading to the Same Product. *Chem. Mater.* **2006**, *18* (11), 1196−1205.

(11) Michailovski, A.; Grunwaldt, J.-D.; Baiker, A.; Kiebach, R.; Bensch, W.; Patzke, G. R. Studying the Solvothermal Formation of MoO3 Fibers by Complementary in Situ EXAFS/EDXRD Techniques. *Angew. Chem., Int. Ed.* **2005**, *44* (35), 5643−5647.

(12) Gnanavel, M.; Pralong, V.; Lebedev, O. I.; Caignaert, V.; Bazin, P.; Raveau, B. Lithium Intercalation into the Jarosite-type Hydroxysulfate: A Topotactic Reversible Reaction from a Crystalline Phase to an Inorganic Polymer-like Structure. *Chem. Mater.* **2014**, *26*, 4521−4527.

(13) Zhang, W.; Duchesne, P. N.; Gong, Z.; Wu, S.; Ma, L.; Jiang, Z.; Zhang, S.; Zhang, P.; Mi, J.; Yang, Y. In Situ Electrochemical XAFS Studies on an Iron Fluoride High Capacity Cathode Material for Rechargeable Lithium Batteries. *J. Phys. Chem. C* **2013**, *1*, 11498.

(14) Stöter, M.; Biersack, B.; Reimer, N. Ordered Heterostructures of Two Strictly Alternating Types of Nanoreactors. *Chem. Mater.* **2014**, *26*, 5412−5419.

(15) Evans, J. S. O.; Price, S. J.; Wong, H. V.; O'Hare, D. Kinetic Study of the Intercalation of Cobaltocene by Layered Metal Dichalcogenides with Time-resolved in Situ X-ray Powder Diffraction. *J. Am. Chem. Soc.* **1998**, *120* (42), 10837−10846.

(16) Du, G.; Guo, Z.; Wang, S.; Zeng, R.; Chen, Z.; Liu, H. Superior Stability and High Capacity of Restacked Molybdenum Disulfide as Anode Material for Lithium Ion Batteries. *Chem. Commun. (Cambridge, U. K.)* **2010**, *46* (7), 1106−1108.

(17) Road, M. In Situ Intercalation of the Layered Compounds TiS2, ZrSe 2 and V g e 2. *Surf. Sci.* **1995**, *333*, 419−424.

(18) Permien, S.; Indris, S.; Scheuermann, M.; Schürmann, U.; Mereacre, V.; Powell, A. K.; Kienle, L.; Bensch, W. Is There a Universal Reaction Mechanism of Li Insertion into Oxidic Spinels: a Case Study Using MgFe 2 O 4. *J. Mater. Chem. A* **2015**, *3* (4), 1549−1561.

(19) Merrill, D. R.; Sutherland, D. R.; Ditto, J.; Bauers, S. R.; Falmbigl, M.; Medlin, D. L.; Johnson, D. C. Kinetically Controlled Site-Specific Substitutions in Higher-Order Heterostructures. *Chem. Mater.* **2015**, *27* (11), 4066−4072.

(20) Lin, J. C.; Sharma, R. C.; Chang, Y. A. The Pb-Se (lead-selenium) system. *J. Phase Equilib.* **1996**, *17*, 253−260.

(21) Okamoto, H. Se-Sn (Selenium-Tin). *J. Phase Equilib.* **1998**, *19*, 293.

(22) Hirota, T.; Ueda, Y.; Kosuge, K. Phase diagram of the $TiSe_x$ system ($0.95 \leq x \leq 2.00$). *Mater. Res. Bull.* **1988**, *23*, 1641−1650.

(23) Aykol, M.; Dwaraknath, S. S.; Sun, W.; Persson, K. A. Thermodynamic limit for synthesis of metastable inorganic materials. *Science Advances* **2018**, *4*, No. eaaq0148.

(24) Atkins, R.; Wilson, J.; Zschack, P.; Grosse, C.; Neumann, W.; Johnson, D. C. Synthesis of [(SnSe) 1.15]m((TaSe2)n Ferecrystals: Structurally Tunable Metallic Compounds. *Chem. Mater.* **2012**, *24*, 4594−4599.

(25) Phung, T.; Jensen, J.; Johnson, D.; Donovan, J.; McBurnett, B. Determination of the Composition of Ultra-thin Ni-Si Films on Si: Constrained Modeling of Electron Probe Microanalysis and X-ray Reflectivity Data. *X-Ray Spectrom.* **2008**, *37*, 608−614.

DOI: 10.1021/jacs.8b10681
J. Am. Chem. Soc. 2019, 141, 922−927